Trapped Gas, Relative Permeability and Residual Oil Saturation of an Oil-Wet Sandstone[1]

J.G. Kralik, L.J. Manak, A.P. Spence, and G.R. Jerauld, ARCO

Abstract

An experimental dataset from preserved reservoir sandstone is used to demonstrate features important to oil-wet systems not usually included in three-phase relative permeability models. They are described by a generalized version of the relative permeability model developed by Jerauld (1997).

The sandstone reservoir studied shows large amounts of spontaneous imbibition of oil and traps water during secondary drainage. Oil relative permeability is almost a function of oil saturation alone while water relative permeability is significantly lower in the presence of trapped gas. The trapped gas level depends on the relative amounts of oil and water. While two-phase trapped gas values are consistent with values in the literature for similar sandstones, three-phase trapped gas levels are approximately half of two-phase levels. Residual oil saturations after waterflooding and gasflooding followed by waterflooding are roughly the same. Furthermore, the incremental oil production during a waterflood following gasflooding was minimal. Experiments run with different pressure drops show that the low trapped gas saturations are not due to capillary desaturation. CT scans show that little redistribution of gas occurs during trapping.

Introduction

While much progress has been made in understanding two-phase flow for nonwater-wet systems, the approaches to treating native-state systems in three-phase flow are lacking. Current approaches to three-phase flow in commercial simulators and laboratories are largely based on water-wet systems. It is clear, however, that wettability should affect aspects of three-phase flow. Advances in understanding how wettability affects three-phase flow have been impeded by a lack of high-quality data. This paper presents data on a naturally oil-wet system that demonstrates many features important to three-phase flow. While many of these are not new, many are not well established. To our knowledge there are no data sets covering the combination of circumstances addressed here.

The data reported were taken to understand the incremental oil recovery of immiscible and miscible water-alternating-gas (IWAG & MWAG) processes over waterflooding. Because the production of oil in the field of interest is limited by gas handling and, for conservation reasons, produced gas must be reinjected, the amount of gas trapped by various processes is equally important. Corefloods showed that residual oil saturation to waterflooding is minimally affected by the presence of trapped gas and therefore, unlike MWAG, IWAG is ineffective at increasing oil recovery. Trapped gas experiments done on extracted cores at room conditions and on preserved core after miscible flooding gave results similar to each other and other sandstones of similar porosity reported in the literature. However, the trapped gas measured in three-phase flow is half that measured in two-phase flow. Consequently, MWAG is differentially better as both an oil recovery and a gas storage process.

Two lithologies are discussed in this paper, the A- and C-sands. The A-sand consists of very fine- to fine-grained, moderately to well sorted, quartzose sandstone deposited in a shallow marine environment. The C-sand consists of fine-grained to pebbly, bioturbated, poorly sorted, glauconitic sandstones deposited in a shallow marine environment.

Trapped Gas. Figure 1 shows a comparison of gas saturation trapped by water (S_{gt}) measured on extracted C-sand plugs at room conditions with ones on fresh plugs with residual oil to miscible flood (S_{orm}), as well as data measured on preserved core in three-phase (3ϕ)

Figure 1 Trapped gas data for C-sand. Three-phase data is from zone C3 and is 60% of two-phase values.

immiscible flow at reservoir conditions. The data show that while S_{gt} does depend strongly on maximum gas saturation (S_g^{max}), S_{orm} does not change S_{gt} within experimental uncertainty. However, the S_{gt} measured in 3ϕ flow is lower than that measured in 2ϕ flow. At the same S_g^{max}, the 2ϕ system has a S_{gt} of roughly 20% while the 3ϕ value is 13%. Differences between zones do not explain the observation because 2ϕ data from zones C1, C3 and C4 appear to be the same but different from 3ϕ data from C3.

Figure 2 shows the same comparison for the A-sand. S_{gt} data were measured on extracted plugs at room temperature and on preserved core in 3ϕ flow at reservoir conditions. Again, S_{gt} depends strongly on S_g^{max}. However, S_{gt} measured in 3ϕ flow is significantly lower than in 2ϕ flow. At $S_g^{max}{\sim}25\%$, the 2ϕ $S_{gt}{\sim}22\%$ whereas the 3ϕ $S_{gt}{\sim}11\%$. Differences between subzones do not explain the observation because the 2ϕ data from zone A3 appear to be the same as those for zone A4, but are different than the 3ϕ data. Also shown are the results of a miscible flood conducted on a preserved composite core where S_{gt} is consistent with the 2ϕ data. The experiment consisted of a continuous, gravity-stabilized, multi-contact miscible displacement followed by a waterflood.

Because the various experiments were performed on different samples, the
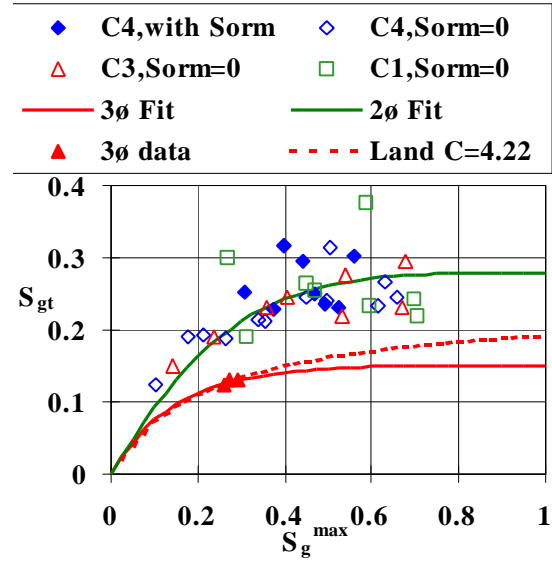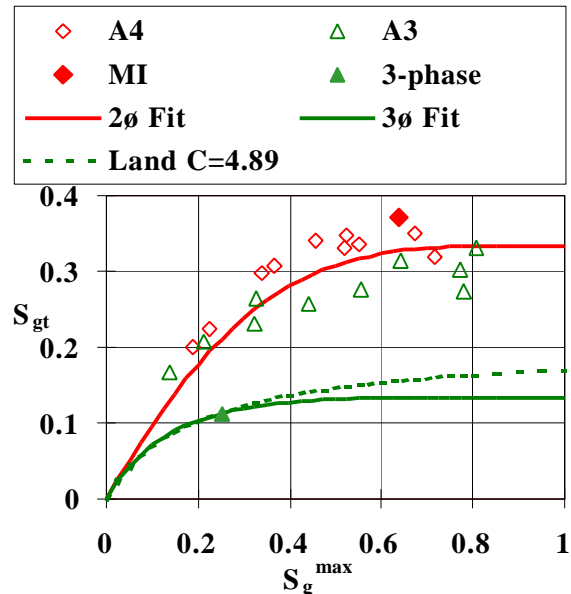

Figure 2 Trapped gas vs. maximum gas for the A-sand. Three-phase data is 50% of two-phase values. The data labeled MI was generated at the end of a miscible flood and has S_{orm}=12.3%.

lithological impact on S_{gt} was evaluated further by comparing the dataset to existing literature. Three major factors influence the level of S_{gt}, S_g^{max}, the porosity, and the level of microporosity (Jerauld 1996). S_g^{max} was eliminated as a parameter in the analysis by fitting the data from each sample to a zero-slope Land curve (Jerauld 1996) and to correlating the maximum trapped gas, i.e. S_{gt} for S_g^{max}=1, with other properties. The current 2ϕ data and data from other sandstones correlate with porosity level (Figure 3). The A-sand data are well within the scatter of data from other sandstones. The C-sand data trend below average because of higher microporosity levels. The agreement between the current and historical S_{gt} data implies that the lower 3ϕ S_{gt} values are not lithological effects.

Figure 3 Maximum trapped gas vs. porosity level for extracted samples compared to literature values.

Experimental

Fluids. Live oil (LO) was made by adding the appropriate light ends to anaerobic stock tank oil (ASTO) to match a bottom hole sample composition. Brine (STB) was made by adding salts (2.56% TDS) to filtered (0.20 µm), degassed deionized water. The STB was stored anaerobically. Live brine (LB) was made by multiple contacts with equilibrium gas at 155°F at the bubble point, 2700 psi. The equilibrium gas composition was obtained from the gas phase produced from a constant composition expansion of the LO to ~10 psi below its bubble point. The pertinent fluid properties are in Tables 1-3.

Screening Plugs. The A-Sand plugs were cut on location from a 10.2-cm low invasion core with connate water saturation of less than 10%. These plugs were taken from the interior of the core using ASTO as the plugging fluid and were stored under ASTO in sealed jars. The 10.2-cm C-Sand core was cut with bland water-based mud and
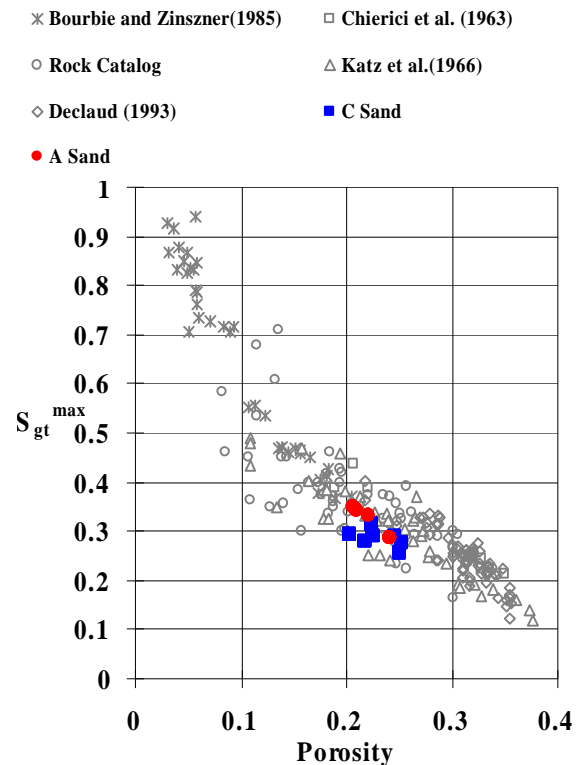
Table 1 Fluid Properties

Fluid	T (°F)	P (psia)	r (g/cc)	m(cP)
STO	160	515	0.8790	8.494 ± 0.029
STB	72	15	1.0151	0.953 ± 0.016
LO	160	2770	0.7994	2.384 ± 0.065
LB	160	2770	0.9856	0.427 ± 0.010

Table 2 Live fluid properties at 155°F for CT-scanned of Composite C. The live oil was doped with 2.2 mass % iodonaphthalene to increase its CT number to that of live brine.

Property	Oil	Brine	Gas
B_i (cc/cc, at 60°F, 1 atm)	1.219	1.032	5.83E-3
R_{si} (cc/cc, at 60°F, 1 atm)	79.72	2.50	
μ_i (cP)	2.384	0.427	0.0185
ρ_i (g/cc at 60°F, 1 atm)	0.9259	1.016	6.52E-3

was assumed to be invaded. Plugs were cut from the interior of preserved core using anaerobic synthetic brine as the plugging fluid. The plugs were preserved under anaerobic plugging fluid and sealed. Both sets of core plugs were

Table 3 Typical Live Fluid Properties at 158°F and 2755 psia

Property	Oil	Brine	Gas
B_i (cc/cc, at 60°F, 1 atm)	1.213	1.032	5.65E-3
R_{si} (cc/cc, at 60°F, 1 atm)	76.9	2.72	
ρ_i (g/cc at 60°F, 1 atm)	0.9158	1.016	6.42E-3

CT-scanned to assess internal heterogeneities. Because the C-Sand plugs were invaded, they were also flushed with roughly 10 pore-volumes (PV) of anaerobic synthetic brine (STB) until a stable ΔP was obtained. The plugs were then centrifuged under argon at a gas-water capillary pressure of 120 psi to establish an immobile water saturation (S_{wi}). All plugs were screened for $k_o(S_{wi})$ using ASTO at reservoir temperature (155°F) and 500 psig pore pressure. Each composite was constructed from those plugs that were geologically and mineralogically consistent, the most homogeneous and possessed the most similar $k_o(S_{wi})$ values. For Composite A, the A-Sand composite, the five plugs had screening $k_o(S_{wi})$ values that ranged from 71 to 117 md. The four plugs in Composite C, the C-Sand composite, had screening $k_o(S_{wi})$ values that ranged from 360 to 428 md.

Composite Construction. Each composite was formed by stacking the plugs end-to-end between the coreholder end-butts. The assembly was wrapped with Teflon tape, then with lead foil that was soldered to provide a gas-tight seal. This assembly was slipped into a Viton sleeve that was wired to the endbutts. The composite assembly was inserted into the coreholder and sealed. Overburden pressure was applied by filling the annulus between the sleeve and coreholder body with a heavy mineral oil. Next, each composite was displaced with several PV of ASTO at 155°F against a 500 psig backpressure until a constant $k_o(S_{wi})$ was obtained for the composite. After soaking overnight, injection was restarted until a constant $k_o(S_{wi})$ was achieved. This process was repeated until the $k_o(S_{wi})$ change was within 5%. After all the tests were complete, each composite was extracted and its routine properties were measured. Composite A had a length of 25.41 ± 0.01 cm, diameter of 3.80 ± 0.02 cm and an air permeability of 105 md. Composite C had a length of 24.95 ± 0.02 cm, a diameter of 3.81 ± 0.03 cm and an air permeability of 622 md.

Sequence of Experiments. After two waterfloods at 12 and 0.5 ft/day, Composite A was gasflooded (GF3) and subsequently waterflooded (WF3). Composite C was waterflooded once (WF1) and then subjected to a series of 3 trapped gas experiments. Because the brine was undersaturated in the first waterflood to S_{gt} (WF2) it was repeated with fresh live fluids and at lower rates to assess if the low S_{gt} value was due to capillary desaturation. The final experiment (GF4/WF4) on Composite C was CT-scanned at flood endpoints to determine if gas redistributed within the composite during the waterflood.

Relative permeabilities were obtained by applying the JBN method and are referenced to the highest $k_o(S_{wi})$. For waterfloods, oil production, and pressure drop across the composite as a function of throughput were measured directly. In the gasflood and subsequent waterflood it was necessary to flash the effluent through a backpressure regulator (BPR). Although ΔP data were still collected essentially continuously, oil

production data consisted of a limited number of discrete aliquots (~10 after breakthrough). Therefore, oil production and pressure drop were fit to stretched exponentials before JBN analysis.

Waterfloods. A STO tracer test was conducted to measure the initial volume of oil in the composite, at 155°F and 500 psig. The test consisted of first displacing the composite with 5 to 6 PV of ASTO traced with 100 ppm trichlorobenzene and then displacing with untraced ASTO. Appropriate integration of the two dispersion curves yielded the oil volume. Next, the composite was displaced with LO at 155°F against a backpressure ~100 psi above the LO bubble point until a constant ΔP was attained. After soaking overnight the LO flush was repeated. The soak-inject cycle was continued until $k_o(S_{wi})$ agreed to within 5% from one cycle to the next.

The waterfloods were limited to 12 to 15 PV of LB injection. During the waterflood, oil production was measured directly with an optical cell immediately downstream from the composite. An acoustical separator downstream from the optical cell served as backup and cumulative oil production monitor. After the waterflood, a tritiated LB tracer test was conducted to measure the water volume. The procedure was similar to that used for the STO tracer test, except the backpressure was ~25 psi above the bubble point.

To establish S_{wi} prior to the next experiment (either WF or GF), the composite was blown down to ambient pressure after cooling. The STO and STB produced were measured. The composite was then heated to 155°F and ASTO was injected against a 500 psig backpressure. Produced brine was collected in a centrifuge tube and its mass measured. Once bulk brine production ceased, STO was recirculated through the composite continuously until water production entirely ceased (7 to 14 days). The STO in the purge stream was analyzed to ensure that additional brine was not being removed by emulsification. Once S_{wi} was established, a STO tracer test was performed to quantify the volume of oil in the composite.

Gasfloods. The composite was prepared in the same way as waterflooding. Gas was injected vertically downward at 2.5 ft/day with pore pressure ~10 psi above the LO bubble point. The composite effluent was flashed through a BPR into a series of tared separators. Cumulative gas production was measured with a wet test meter. After gas breakthrough, the gas rate was increased to 15 ft/day. Gas injection continued until oil production effectively ceased. A final gas permeability measurement was made with the gas injection rate at 2.5 ft/day.

Waterfloods to S_{gt}. Following the gas flood, the coreholder was rotated 180° to allow water injection vertically upward. Initially, gas was injected vertically upward at the same rate used for the waterflood until a stable ΔP and gas production rate were attained. Simultaneously, gas injection ceased and brine injection commenced. The effluent was flashed through a BPR into a series of sealable, centrifugable vials. Cumulative gas production was measured with a wet test meter. Total LB throughput was limited to ~4 PV at a pore pressure 10 to 20 psi above the LB bubble point. A LB tracer test was then conducted to measure the volume of LB in the composite in the presence of trapped gas.

The composite was then cooled and blown down with the masses of STO and STB and the volume of gas produced measured. The composite was then resaturated with STB at ambient temperature and a tracer test conducted to determine the volume of STB in the composite.

CT-Scanned Waterflood to S_{gt}. Composite C was dismounted from its original coreholder and placed intact in a CT-scannable aluminum coreholder. Assembly was essentially the same as for the conventional waterfloods except that the lead foil was replaced by nickel foil. General procedures for conducting the experiment were the same as those described above.

To maximize the resolution of the CT data in terms of S_g, the LO was doped with an x-ray adsorber to match the CT number (N_{CT}) of the LB. Initially, iodo-decane was used to increase the LO N_{CT}. However, a stable N_{CT} could not be obtained during the doped LO displacement even after 10 PV of injection. STO dispersion curves suggested the undoped LO displacement should have been complete after approximately 3 PV. This observation suggested that iododecane was unstable at reservoir conditions, which was confirmed in an independent study. A consequence of the iododecane breakdown was the uptake of I^-(aq) by the connate water, which led to an increase in its N_{CT}. Iodonaphthalene was found to be stable at reservoir conditions and was used at a concentration of 2.2 mass % in the LO. Equation of state (EOS) calculations predicted the original solution gas synthesized through propane would strip sufficient intermediates from the LO to increase the density by 7% after 8 contacts. To mitigate stripping of the LO, the equilibrium gas composition was matched through C_6. The predicted increase in density fell to 3% after 8 contacts.

CT scans were obtained at the start and end of the gasflood, at liquid breakthrough, the end of the waterflood and after the waterflood bump. At the end of the experiment, the composite was cooled to ambient temperature and blown down. The produced fluids were measured and a STB tracer test conducted. The brine was removed by methanol displacement. The methanol effluent was analyzed for water using Karl-Fischer titration. Correcting the water recovered for the salt content of the brine, the volume of STB removed from the composite was 61.2 ± 0.1 cc which agrees with the STB tracer test value of 60.6 ± 0.8 cc. A chloroform flush removed the residual oil. Baseline scans at 100% gas saturation and 100% LB saturation completed the data acquisition.

Results
Wettability. This system is among the most oil-wet that the authors have encountered but is best classified as weakly oil-wet. Amott indices measured on 4 adjacent plugs for each lithology yielded average values for the A-sand I_w=0.02, I_o=0.48 and for the C-Sand I_w=0.03 and I_o=0.30. The Amott tests were performed on preserved samples at reservoir temperature with STO and synthetic reservoir brine. Oil-based core data and 2ϕ gas-oil and mercury injection capillary pressure data show good agreement on a J-function basis indicating that the origin of the oil-wet behavior is the Salathiel (1973) mechanism.

Contact angle measurements made with live reservoir crude and simulated formation brine on quartz at reservoir temperature and pressure show water receding contact angles

in the range of 25º-35º and water advancing contact angles in the range of 90º-160º. Systems with water-advancing contact angles above 150º are generally called oil-wet, between 110º and 150º weakly oil-wet and between 70º and 100º intermediate-wet. Thus, this system is weakly oil-wet. Water-oil interfacial tension measurements made with the same fluids indicate γ_{ow}=35±0.3 dynes/cm. At the bubble point, γ_{go}=5.7 dynes/cm was estimated from EOS calculations and Parachors. The Firoozabadi and Ramey (1988) correlation predicts a gas-water interfacial tension of 57 dynes/cm. If these interfacial tensions are accurate, oil will spread on the gas-water interface and the effective gas-water interfacial tension is actually 5.7+35=40.7 dynes/cm. Based on the relation (Zhou and Blunt, 1997), $\gamma_{gw}\cos\theta_{gw}= \gamma_{go}\cos\theta_{go}+ \gamma_{ow}\cos\theta_{ow}$, and the assumption that the gas-oil contact angle is zero, gas-water contact angles can be estimated. If water is advancing, the gas-water contact angle is in the range 82º-132º, which is intermediate to very weakly gas-wet. When water is receding the contact angle is in the range of 23-32º and gas is nonwetting to both water and oil.

This implies that in a gasflood, k_{rg} should be roughly the same as in a water-wet system whereas in a waterflood, gas should be intermediate-wet. Trapped gas in an intermediate-wet system should be smaller because choke-off is inhibited. Model systems show no choke-off for advancing contact angles >70º (Li and Wardlaw, 1986). This explanation is similar to that for water-oil systems in which S_{orw} is lower for intermediate-wet systems than water-wet systems (Jadhunandan and Morrow 1995). Implicit in this explanation is the idea that water traps gas and therefore no oil bank forms, as was observed.

Waterfloods. Tables 4 and 5 contain the endpoint saturations and permeabilities for all tests for Composite A and C, respectively. Both composites demonstrated oil-wet behavior during the waterfloods, as evidenced by the relatively high remaining oil saturations after 12 PV of throughput and the very slow approach of the oil fractional flow to zero. In a parallel study, the S_{orw} endpoints of centrifuge water-oil imbibition capillary pressure measurements were 28% for the A-Sand and 16% for the C-Sand.

Because Composite A consisted of uninvaded core, it was possible to acquire true primary imbibition k_{row}-k_{rw} curves. Since S_{wc} was only 8%, it is very difficult to restore. The subsequent recirculating STO drive only reduced S_w to 21%. The k_{row}-k_{rw} curves for both WF1 and WF2 are given in Figure 4, which shows that $k_o(S_{wi})$ for WF2 lies on the primary imbibition k_{row} curve from WF1. This demonstrates the difficulty in obtaining reliable $k_o(S_{wi})$ from water-invaded core. WF2 was conducted vertically upward at 0.5 ft/day to mitigate gravity effects. Significant capillary

Table 4 Endpoint data for Composite A. Flowrate u_i is in ft/day (total PV), k_i in md, residual phases in percent.

	u_i	$S_{wi}(wf)$	$S_{or}(wf)$	$S_{gr}(wf)$	k_i
OF1		8 ± 1			92 ± 5
WF1	12		39 ± 2		28 ± 1
OF2		21 ± 2			29 ± 2
WF2	0.5		47 ± 2		4.7 ± 0.2
WF2	12		40 ± 2		19.4 ± 0.5
WF2	23	bump	38 ± 2		23.4 ± 0.6
OF3	3	21 ± 2			30.9 ± 1.7
GF3	3		57 ± 3	22 ± 1	6.4 ± 2.3
GF3	18	bump	54 ± 3	25 ± 2	7.7 ± 0.6
WF3	12		40 ± 4	11 ± 9	4.3 ± 0.1

holdup of oil (i.e. capillary end effect) occurred as evidenced by the higher S_{or}(wf) and lower $k_{rw}(S_{or})$. After the rate was increased to match WF1, S_{or}(wf) decreased to that of WF1. Doubling the brine rate again slightly decreased $S_{or}(wf)$ and increased $k_{rw}(S_{or})$.

The k_{row}-k_{rw} curves for the C-Sand waterflood are displayed in Figure 4. The subsequent oildrive reduced S_w to only 36% where $k_o(S_{wi})$ was on trend with the k_{row} curve from WF1.

Gasfloods. Gasflood results were similar for both composites. None of the gasfloods produced any brine. Oil displacement efficiency was marginally better in Composite C than in Composite A.

Waterfloods to S_{gt}. The first experiment, WF3, was conducted on Composite A (Table 4, Figure 4). The cumulative gas production up to the point of liquid breakthrough was unknown so S_{gt} was calculated from the LB tracer test at S_{gt}, the blowdown production and the STB tracer test. Accounting for cumulative uncertainties, S_{gt} was 11±9%.

Table 5 Saturation and permeability data for composite C. BT means liquid breakthrough. Flowrate, u_i, is in ft/day. [1]Trapped gas stripped by undersaturated brine.

	u_i	S_{wi}(wf)	S_{or}(wf)	S_{gr}(wf)	k_i (md)
OF1	10	30 ± 3			362 ± 22
WF1		BT	42 ± 4		
WF1	10	bump	36 ± 4		116 ± 6
OF2	3.2	35 ± 3			314 ± 13
GF2	3.2		43 ± 5	23 ± 3	15 ± 6
GF2	19		40 ± 5	25 ± 3	~ 106
WF2	12	BT	40 ± 5	12 ± 3	
WF2			35 ± 7	~ 3[1]	42 ± 2
OF3	2.4	37 ± 2			300 ± 15
GF3	2.4		43 ± 2	27 ± 1	15 ± 2
GF3	15	bump	39 ± 2	29 ± 1	~ 63
WF3	0.5	BT	39 ± 2	13 ± 1	
WF3	0.5		36 ± 2	13 ± 1	6.5 ± 2
WF3	10	bump	35 ± 2		13.6 ± 0.5
WF3	0.5		35 ± 2	13 ± 1	12.9 ± 0.5
OF4	2.4	37 ± 1			309 ± 3
GF4	2.4		38 ± 1	25 ± 1	3.6 ± 0.3
GF4	14		36 ± 1	27 ± 1	
WF4	0.5	BT	36 ± 1	13 ± 1	
WF4	0.5		35 ± 1	12 ± 1	12.8 ± 1.4
WF4	10	bump	34 ± 1	12 ± 1	17.8 ± 1.1

The presence of trapped gas greatly suppressed k_{rw}. Interestingly, the residual oil saturation after WF1 and WF3 were essentially the same. Unlike results in the literature for water-wet systems, trapped gas did not lead to a reduction in $S_{or}(wf)$ (c.f. Figure 5). Furthermore, the relatively low S_{gt} was not expected based on previous 2ϕ data which, for S_{gi} of 25%, predicted a S_{gt}>20%.

The first gasflood/waterflood sequence on Composite C (GF2/WF2) was inadvertently conducted with depleted fluids. Because, the gasflood was conducted at 2930 psia, the bubble points of the residual oil and brine phases should have been restored. Again, S_{gt} was substantially less than that predicted by the 2ϕ S_{gt} data. After injection of an additional 9 PV of the depleted brine (P_{BP}~2200 psia), S_{gt} was stripped down to ~3%.

The flood was repeated with fresh reservoir fluids. To test the possibility that capillary desaturation was responsible for the low S_{gt}, WF3 was run at 0.5 ft/day instead of 10 ft/day. Even at the lower rate, the cumulative gas production to the point of liquid breakthrough indicated that S_{gt} was 13%. Incremental gas production after liquid breakthrough could be attributed to solution gas. S_o declined from 36 to 33% after liquid breakthrough. Increasing the brine rate to 10 ft/day did not yield any incremental oil or gas production. The presence of the trapped gas resulted in a large reduction in k_{rw}, but
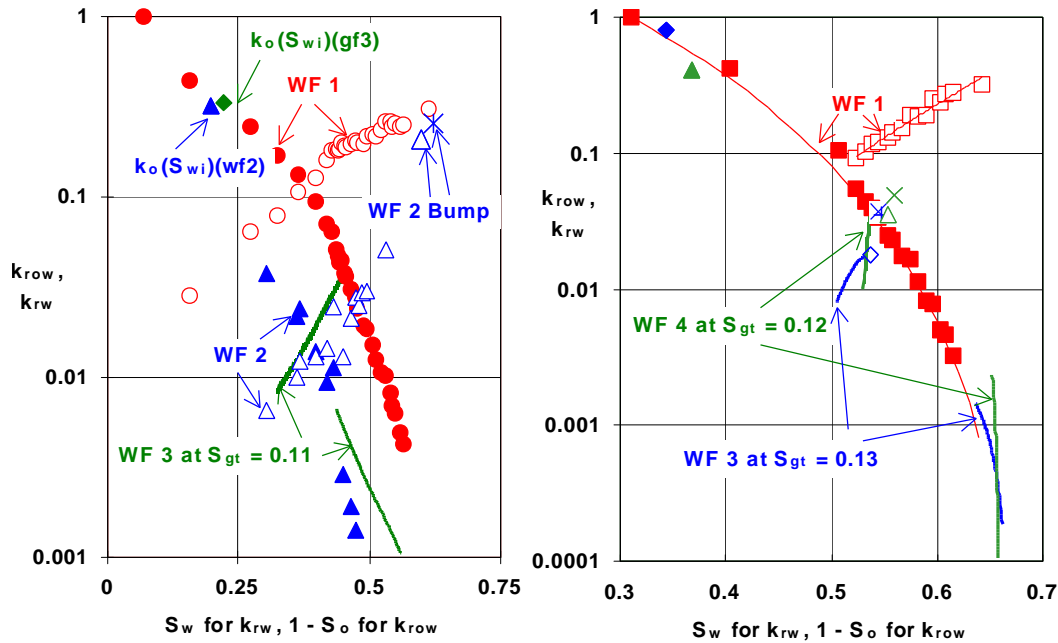
Figure 4 Water-oil relative permeability for Composite A (left) and Composite C (right). A-sand WF1 was conducted at 12 ft/day, WF2 at 0.5 ft/day. A-sand WF3 shows the reduction in k_{rw} due to the presence of S_{gt}. C-sand WF3 and 4 show the reduction in k_{rw} due to the presence of S_{gt}.

had no effect on k_{row}. As with Composite A, S_{gt} had no impact on S_{or}. The low S_{gt} achieved at the lower brine displacement rate argues that capillary desaturation is not responsible. WF3 had a capillary number of $6x10^{-6}$. Chatzis and Morrow (1984) report no change in residual nonwetting phase below this capillary number for continuous or discontinuous phases.

To determine whether the initial gas saturation established in the composite was redistributed during the waterflood, GF3/WF3 was repeated at the same conditions, except the composite was CT-scanned at strategic endpoints during the sequence. Gas trapping and oil recovery were essentially the same as WF3. Scans were made every 5 mm down the composite axis. After each scan, the average CT number (N_{CT}) of each slice was determined in the region of interest which encompassed as much of the rock as possible while staying just inside the core. All CT-based initial gas saturations were normalized with respect to $N_{CT}(S_l=1)–N_{CT}(S_g=1)$ for each slice. $N_{CT}(S_l=1)$ corresponds to the scan prior to the gasflood and $N_{CT}(S_g=1)$ corresponds to the CT scan of the extracted composite saturated 100% with equilibrium gas.

The connate water prior to GF4 was contaminated with I^-(aq), the byproduct of the decomposition of the iodo-decane used
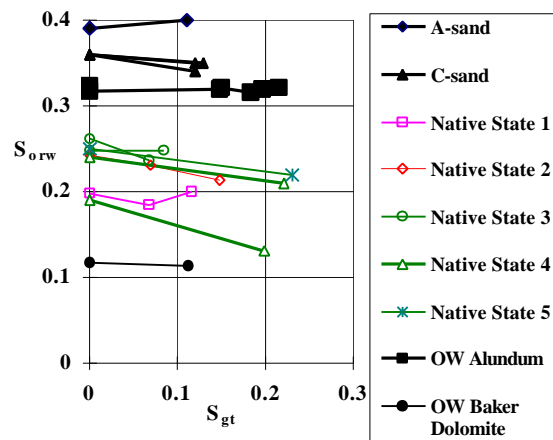

Figure 5 Dependence of residual oil to waterflooding on S_{gt} for A-sand and C-sand compared to oil-wet data from the literature (Kyte et al 1956, MacAllister et al 1993) and for native state data from other reservoirs.

in the initial attempts to dope the LO. Because essentially no gas was produced after liquid breakthrough, N_{CT} should have been constant provided N_{CT} for both liquid phases were the same. $N_{CT}(S_{gt,bt})$ and $N_{CT}(S_{gt})$ did not differ for approximately the first 75% of the composite, but then diverged. At the point of liquid breakthrough, I^- contaminated connate water was still in the composite. After the waterflood, however, the connate water had been flushed from the core. This was confirmed when the initial 0.59 g of STB produced was found to contain 6030 ppm I^-(aq). Analysis of the injected brine found no detectable iodide. Using the last 5 slices, $N_{CT}(S_{gt,bt})>N_{CT}(S_{gt})$ by 16.1 ± 1.9 CT numbers. This 16.1 CT numbers was assumed to be the offset to the 100% liquid saturated core scans due to iodide in the connate water. Therefore, $N_{CT}(S_l=1)$ was decreased by 16.1 as the baseline for calculating S_{gt}. Applying this correction, integration of the $N_{CT}(S_{gt})$ data yielded $S_{gt,CT}$=12.6% vs. $S_{gt,MB}$ =12.2%, based on material balance.
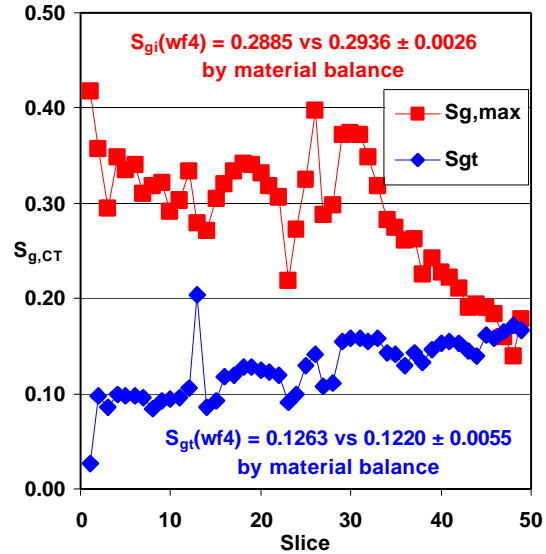

Figure 6 S_{gi} and S_{gt} for each slice calculated from calibrated NCT data. Each datum corresponds to the average gas saturation for each 5 mm thick slice of the composite. Slice 1 is the inlet. There is good agreement between the material balance and CT data.

The gas saturation profile along the length of the composite is plotted in Figure 6 for S_{gi} and S_{gt}. S_{gi} was highest at the inlet, remained relatively constant for the first 75% of the composite, then declined from 27% to 16% through the final plug. S_{gt} was 3% at the inlet, jumped rapidly, then rose linearly to 16% at the outlet. If the N_{CT} data for the first three plugs in the composite are integrated $S_{gi,CT}$=31.8% and $S_{gt,CT}$=11.7%, similar to the whole composite values. Integration of the N_{CT} data for the final plug in the composite however, yield $S_{gi,CT}$=19.7% and $S_{gt,CT}$=15.4%, more consistent with the 2ϕ data.

Three-phase Relative Permeability Model

The relative permeability model used to assess the impact of these observations is a generalized form of the one described by Jerauld (1997). The original form of this model included a gas relative permeability (k_{rg}) function that depended on both gas and water saturation rather than just gas saturation. However, this form was dropped because available data did not justify its use. The model was developed for a mixed-wet system that did not show significant water trapping. Water trapping was added here.

Other studies have found that the k_{rg} depends on two saturations. For intermediate-wet Yegua and water-wet Frio sand, Schneider and Owens (1970) report that drainage k_{rg} is greater at connate water than at residual oil saturation. However, they found no differences for oil-wet Tensleep sandstone. Berry et al (1992) reported that gas-water relative permeability was smaller than gas-oil relative permeability. Skauge and Larsen (1994) reported data that show both k_{rg} and k_{rw} depend on two saturations and are lower for 3ϕ flow than 2ϕ flow. Empirical relative permeability models reported by Houstad

and Hansen (1995) and Blunt (1998) have k_{rg} that depend on two saturations. Some simulators have also included a "water repellant" option in which gas is intermediate wetting, oil is wetting and water is nonwetting.

Gas Relative Permeability. k_{rg} is modeled similarly to the k_{ro} function used by Jerauld,

$$K_{rg} = K_{rgg}\left(S_g\right)\frac{K_{rgo}\left(1-S_o-S_{wch}\right)K_{rgw}\left(1-S_w\right)}{K_{rgg}\left(1-S_o-S_{wch}\right)K_{rgg}\left(1-S_w\right)} \qquad \text{with} \qquad K_{rgg}\left(S_g\right)=\frac{\left(1+c_{gg2}\right)S_{gg}^{c_{gg1}}}{\left(1+c_{gg2}S_{gg}^{c_{gg1}(1+1/c_{gg2})}\right)}$$

$$S_{gg}\left(S_g\right)=\frac{S_g-S_{gt}\left(S_g^{max}\right)}{1-S_{ggr}-S_{wch}} \quad \text{and} \quad S_{gt}=\frac{S_g^{max}}{1+\left(\dfrac{1-S_{wch}-S_{gt}^{max}}{S_{gt}^{max}}\right)\left(\dfrac{S_g^{max}}{1-S_{wch}}\right)^{1+S_{gt}^{max}/\left(1-S_{gt}^{max}-S_{wch}\right)}}$$

where the 2ϕ gas-oil and gas-water relative permeabilities (K_{rgo} and K_{rgw}) have the same form as the 3ϕ function but with different parameters ($c_{ggi}\rightarrow c_{goi}$ and $c_{ggi}\rightarrow c_{gwi}$). Likewise, the 2ϕ trapped gas function has the same form as the 3ϕ function but different parameters. The 2ϕ functional form is the same as that used in the past. When the parameters in the 2ϕ and 3ϕ functions are equated, k_{rg} is just a function of gas saturation. The parameters in k_{rg} vary with composition in a complementary way to k_{ro} so that relative permeability varies appropriately with composition and as miscibility is approached (Jerauld 1997). Because only drainage gas-oil k_{rg} data were available, only these data and S_{gt} were used to determine the parameters in the function.

Water-Trapping. Because this system is oil-wet, water trapping may be an operative mechanism. This behavior has been reported in floods in carbonates (Schneider and Owens, 1976). Figure 7 shows data from preserved A-sand cores that demonstrate this effect. Water trapping in an oil-wet system is similar to gas trapping. During secondary drainage, k_{rw} is smaller than during primary imbibition but k_{rw} is the same in secondary imbibition and secondary drainage. k_{row} is the same for both drainage and imbibition as expected in an oil-wet system. The amount of trapped water found from low invasion cores is shown in Figure 8. This figure also shows the relationship between trapped water saturation and maximum water saturation used in modeling. Because there are few data available, the same functional form as that for
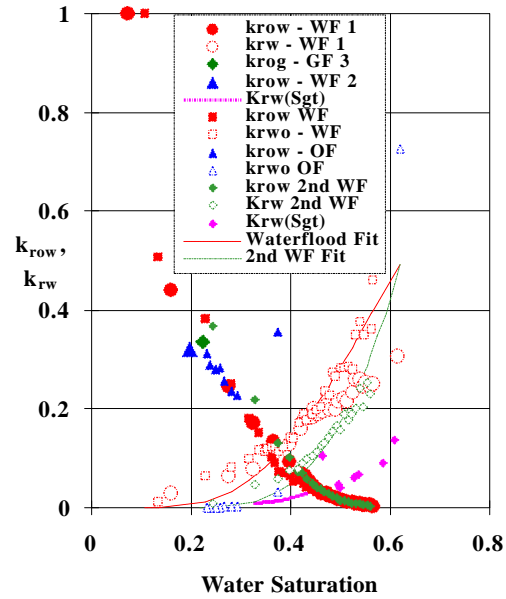

Figure 7 Data showing hysteresis behavior and impact of trapped gas in A-sand relative permeability data. Fit demonstrates how the hysteresis behavior is modeled.

trapped gas was used. However, instead of depending on maximum water saturation this function was assumed to depend on the difference between maximum water saturation and the connate water saturation. The parameter determined from the maximum level of trapping was $S_{wto}^{max}=0.114$. The water-oil relative permeability function is

$$K_{rwo} = \frac{(1+c_{wo5})\left(\dfrac{S_w^{max}-S_w^{min}}{1-S_w^{min}}\right)^{c_{wo4}}}{\left[1+c_{wo5}\left(\dfrac{S_w^{max}-S_w^{min}}{1-S_w^{min}}\right)^{c_{wo4}}\right]}\left(\frac{S_w-S_{wto}}{S_w^{max}-S_{wto}}\right)^{c_{wo3}}$$

with the trapping function

$$S_{wto} = S_w^{min} + \frac{\left(S_w^{max}-S_w^{min}\right)}{1+\left(1/S_{wto}^{max}-1\right)\left(S_w^{max}-S_w^{min}\right)^{1/\left(1-S_{wto}^{max}\right)}}$$

Figure 8 Data from uninvaded core showing the relationship between trapped and maximum S_w.

Three-phase k_{rw} is taken to be the saturation-weighted average of water-oil and water-gas relative permeability. Because k_{rwg} is smaller than k_{rwo}, this reduces k_{rw} appropriately in the presence of gas.
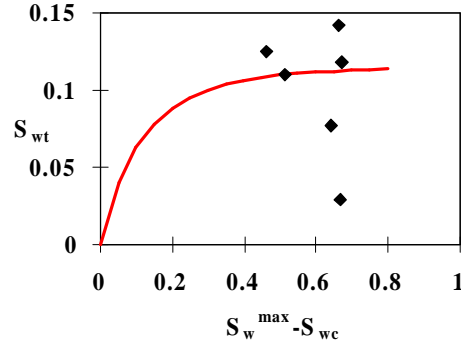
Simulations

Fully compositional type pattern simulations were performed using two C-sand models to assess the impact of the lower trapped gas and water trapping on WAG floods. Both models are two-dimensional injector producer pairs with varying cross-section to emulate the change in velocity that occurs in a 5-spot on 160 acres spacing. One model was a layer-cake model developed to model IWAG/MWAG processes. This model has a layer thickness that ranges from 2 to 8 ft and is 9 layers thick and 80 gridblocks long. Horizontal permeability ranges from 110 to 1640 md and average 450 md. Vertical permeabilities range from 0.03 to 725 md and average 110 md. Porosity ranges from 0.22 to 0.34 and average 0.26. Water saturations ranged from 0.16 to 0.40 and average 0.28. The second model contains a more stochastic description. It consists of 41 layers with thickness in the range of 0.9 to 1.6 feet and 68 gridblocks in the x-direction. Horizontal permeability ranges from 0.1 to 1000 md, vertical permeability varies from 0.01 to 200 md, porosity varies from 0.03 to 0.26, and the initial water saturation is 0.15. Both models were run at constant production rate and constant pressure. A 12-component EOS characterization was used for all of the simulations. The lean gas contains more than 85% methane. The miscible injectant is made by adding natural gas liquids and has a minimum miscibility pressure equal to reservoir pressure.

In the stochastic model, four kinds of gas flooding processes were performed, ordinary IWAG, IWAG with the last few cycles replaced by miscible WAG (IMWAG), lean gas chase - IWAG with the first few cycles replaced by MWAG (MIWAG) and a simple large slug MWAG. Ten cycles consisting of 90 days of gas and 200 days of water were used. The amount of immiscible gas was a 24% hydrocarbon pore-volume slug. The mixed cases consisted of 17.4% HCPV of lean gas and 5.6%HCPV miscible gas. The miscible flood used a 20% HCPV slug of miscible injectant. The flood rate was roughly 6.4% HCPV per year.

A subset of these cases, consisting of IWAG, and IMWAG were run in the layer-cake model. In the IWAG case, a 15% HCPV gas slug was used whereas a 14.2% HCPV slug was used in the IMWAG case (2 cycles of lean gas followed by 1 cycle of miscible gas). WAG cycles consisted of 100 days of gas followed by 100 days of water. The flood rate was roughly 20% HCPV/year. Table 6 shows a summary of the final oil recoveries and retained gas levels at a water-oil ratio of 30. The results indicate that lower trapped gas does not change the oil recovery appreciably but does lower the retained gas. However, the amount of lowering is smaller than input. Rather than being 40% lower the retained gas is 35% lower in the case of IWAG and 28% lower in the case of MWAG following IWAG. The oil incremental recovery is 0.6% OOIP smaller with a lower trapped gas in the MIWAG case.

Table 6 Summary of results for the layer-cake model. Oil recovery is in fraction OOIP as is retained gas. S_{gt3} indicates lower three-phase trapped gas, S_{wt} indicates trapped water.

	Oil Recovery			Retained gas	
	WF	**IWAG**	**IMWAG**	**IWAG**	**IMWAG**
Base	0.448	0.442	0.468	0.111	0.109
S_{gt3}	0.448	0.440	0.462	0.072	0.078
S_{gt3},S_{wt}	0.451	0.446	0.465	0.076	0.081

Table 7 shows the similar results for the stochastic model. The magnitudes of the changes relative to the layer-cake model are different; i.e., the results are description dependent. While in the layer-cake model, using the lower level of trapped gas in 3ϕ flow during IWAG decreases the retained gas by 35%, in the stochastic model the retained gas is lowered by 21%. Similarly, in the case of IMWAG, the retained gas is lowered by 28% in the layer-cake model and only 14% in the stochastic model.

Table 7 also shows that the level of gas retention in the miscible cases is strongly impacted by phase partitioning as well as immiscible trapping. MWAG is only affected by 9% when the 3ϕ trapping function is reduced whereas the IMWAG decreased by 14%. The MIWAG base case has the most gas trapping. However, MIWAG exhibits more of a dependence on the amount of gas retained on the 3ϕ trapping function, declining by 19% when it is lowered. The IWAG case is the most affected by the 3ϕ trapping function, decreasing by 21%.

Table 7 Summary of results for the stochastic model. S_{gt3} indicates lower three-phase trapped gas, S_{wt} indicates trapped water.

	Oil Recovery, fraction OOIP					Retained Gas, fraction OOIP			
	WF	**IWAG**	**IMWAG**	**MIWAG**	**MWAG**	**IWAG**	**IMWAG**	**MIWAG**	**MWAG**
Base	0.406	0.411	0.431	0.422	0.493	0.105	0.109	0.115	0.109
S_{gt3}	0.406	0.404	0.434	0.429	0.462	0.083	0.094	0.093	0.099
S_{gt3},S_{wt}	0.421	0.408	0.431	0.447	0.491	0.087	0.097	0.096	0.102

Discussion

Impact of S_{gt} on S_{orw}. In the literature, the reduction in residual oil saturation has been observed to follow the equation $S_{or} = S_{orw} - a\,S_{gt}$, where the parameter a quantifies the effect. Water-wet data from Holmgren and Morse (1951) and Kyte et al. (1956) suggest that a is roughly 0.5. Kyte et al also reported data for Alundum rendered oil-wet by dri-film that indicate a=0. Skauge (1996) reports 0.5 to 1 for water-wet systems and 1 for weakly water-wet systems. Data reported by MacAllister et al. (1993) for Baker dolomite indicate that a is 0.75, 0.25 and 0.04 for water-wet, mixed-wet and oil-wet conditions respectively. Unpublished in-house data from the 1950's indicate a is 0.59±0.09,

0.51±0.08 and 0.45±0.08 for water-wet, weakly water-wet and intermediate wettability samples respectively. Thus, the current results are generally consistent with those in the literature that indicate less impact (smaller *a*) for more oil-wet systems.

Dependence of S_{gt} on wettability. Schneider and Owens (1976) found that gas trapped by water was 22% in oil-wet native-state San Andres core and 32% after the core was cleaned with polar solvents. Skauge (1996) reports that the Land constant is in the range 1.5 to 2.5 (S_{gt}^{max}=0.40 to 0.29) for water-wet sandstone and 2.25 to 3.5 (S_{gt}^{max}=0.30 to 0.22) for a weakly water-wet sandstone where the range depends on saturation history. MacAllister et al. (1993) reported that S_{gt} depends on wettability and is 11% or less (<40% of water-wet value) for Baker dolomite rendered oil-wet by pickling in crude. All these results indicate that wettability affects trapped gas as observed in the current study.

Dependence of k_{rw} on S_{gt}. Schneider and Owens (1970) showed that for oil-wet Tensleep sandstone and Greyburg carbonate that k_{rw} at a given water saturation decreased with increasing S_{gt}. Schneider and Owens (1976) found the same trend for preserved moderately oil-wet carbonate. MacAllister et al (1993) show trends similar to Schneider and Owens. Jerauld (1997) reported data for mixed-wet sandstone showing a reduction in k_{rw} in the presence S_{gt}. Skauge and Larsen (1994) indicate that k_{rw} is decreased in 3ϕ flow. Thus, $k_{rw}(S_{gt})$ is generally smaller than k_{rwo} for nonwater-wet systems.

Conclusions
The results presented here demonstrate many features important to oil-wet systems.
- Gas trapping depends on wettability and the relative amounts of the other two-phases and can be lower in three-phase flow. This implies that gas relative permeability does not depend on gas saturation alone but on the relative amounts of the other two phases. The results indicate the need to measure trapped gas on native state cores.
- Residual oil to waterflood was unchanged in the presence of trapped gas, consistent with the idea that oil relative permeability is a function of oil saturation alone.
- Water relative permeability depends on the relative amounts of the other two phases and is lower in the presence of gas. It also displays hysteresis and water trapping.

Acknowledgments

Nomenclature
B_i = formation volume factor of phase i, (cc/cc)
I_i = Amott wetting index for phase *i*
k_i =permeability to phase i, md
k_{ri} = relative permeability to phase *i*
K_{rij} = relative permeability for phase *i* w.r.t j
N_{Ca} = capillary number, dimensionless

N_{CT} = CT number, dimensionless
P = pressure, psia
R_{si} = gas to liquid ratio, (cc/cc)
S_i =saturation of phase i, dimensionless
S_{it} =trapped saturation of phase i
S_{ji} =initial saturation of phase j

S_{ir} =residual saturation of phase i
T =temperature, °F
u_i =fluid space velocity of phase i, ft/d
$\boldsymbol{g}$ =interfacial tension, dynes/cm
$\boldsymbol{D}P$ = the pressure drop, psi
$\boldsymbol{q}$ =the contact angle, degrees
μ_i =the viscosity of phase i, cP
ρ_i =the density of phase i, g/cc

Subscripts
CT =related to the CT scanner
BP =bubble point
g =gas
o =oil
w =water
Superscripts
max = maximum

References

Berry, J.F., Little, A.J.H. and Skinner, R.C. 1992 "Differences in Gas/Oil and Gas/Water Relative Permeability," SPE/DOE 24133, 8th Symp. on EOR, Tulsa, OK, April 22-24.

Bourbie, T. and Zinszner, B. 1985 "Hydraulic and Acoustic Properties as a Function of Porosity in Fontainebleau Sandstone*," J. of Geophysical Research* **90** 11524-11532.

Blunt, M. J. 1999 "An Empirical Model for Three-Phase Relative Permeability," SPE 56474, Annual Tech. Conf. and Exh., Houston, Oct. 3-6.

Chatzis, I. and Morrow, N.R. 1984 "Correlation of Capillary Number Relationships for Sandstone," *SPEJ* (Oct.), 555-562.

Chierici, G.L., Ciucci, G.M. and Long, G. 1963 "Experimental Research on Gas Saturation Behind the Water Front in Gas Reservoirs Subject to Water Drive," 6th World Pet. Cong., Proc., Sec. II, Paper 17, Frankfurt (June 19-26).

Delclaud, J. 1992 "Laboratory Measurements of the Residual Gas Saturation," *EUROCAS* 2, London, May.

Firoozabadi, A. and Ramey, H.J. 1988 "Surface Tension of Water-Hydrocarbon Systems at Reservoir Conditions," Journal of Canadian Petroleum Technology, May-June, pp. 41-48

Holmgren, C.R. and Morse, R.A. 1951 "Effect of Free Gas Saturation on Oil Recovery by Water Flooding," *AIME Trans.* **192**, 135.

Houstad, O.S. and Hansen, A.G. 1995 "A Consistent Correlation for Three-phase Relative Permeabilities and Phase Pressures Based on Three Sets of Two-Phase Data," proc. of 8th European Symp. on IOR, Vienna, May 15-17.

Jadhunandan, P.P. and Morrow, N.R. 1995 "Effect of Wettability on Waterflood Recovery for Crude Oil/Brine/Rock Systems," *SPERE*, (Feb.) 40-46.

Jerauld, G.R. 1996 "Gas-Oil Relative Permeability of Prudhoe Bay" *SPERE* (Feb.) 66-73.

Jerauld, G.R. 1997 "General Three-Phase Relative Permeability Model for Prudhoe Bay" *SPERE* (Nov.), 255-263.

Katz, D.L., Legatski, M.W., Tek, M.R., Gorring, L. and Neilsen, R.L. 1966 "How Water Displaces Gas From Porous Media," *Oil and Gas Journal* (January 10), 55-60.

Kyte, J.R., Stanclift, R.J. Jr, Stephan, S.C. Jr., and Rapoport, L.A. 1956 "Mechanism of Water Flooding in the Presence of Free Gas" *Pet. Trans. AIME* **207**, 215-221.

Li, Y. and Wardlaw, N.C. 1986 "The influence of Wettability and Critical Pore-Throat Size on Snap-Off," JCIS 109, 461-472.

MacAllister, D.J., Miller, S.K., Graham, S.K. and Yang, C.T. 1993 "Application of X-Ray CT Scanning to Determine Gas/Water Relative Permeabilities," *SPEFE* (Sept.), 184-266.

Salathiel, R.A. 1973 "Oil Recovery by Surface Film Drainage in Mixed-Wettability Rocks," *JPT* Oct. 1216-1224.

Schneider, F.N. and Owens, W.W. 1970 "Sandstone and Carbonate Two- and Three-Phase Relative Permeability Characteristics," *SPEJ* (March) 75-84.

Schneider, F.N. and Owens, W.W. 1976 "Relative Permeability Studies of Gas-Water Flow Following Solvent Injection in Carbonate Rocks," *SPEJ* (Feb.) 23-30.

Skauge, A. 1996 "Influence of Wettability on Trapped Nonwetting Phase Saturation in Three-phase Flow," 4th International Symposium on Wettability and its' Effect on Oil Recovery, Montpellier, France, Sept.

Skauge, A., and Larsen, J.A. 1994 "Three-Phase Relative Permeabilities and Trapped Gas Measurements Related to WAG Processes," SCA 9421 presented at the Intl. Symp. of the SCA, Stavanger, 12-14, Sept.